Impact of spatial variability in hydraulic parameters on plume migration within unsaturated surficial formations

Léa Pannecoucke, Mathieu Le Coz, Clémence Houzé, Albane Saintenoy, Charlotte Cazala, Chantal de Fouquet

▶ **To cite this version:**

Léa Pannecoucke, Mathieu Le Coz, Clémence Houzé, Albane Saintenoy, Charlotte Cazala, et al.. Impact of spatial variability in hydraulic parameters on plume migration within unsaturated surficial formations. Journal of Hydrology, 2019, 574, pp.160-168. 10.1016/j.jhydrol.2019.04.016 . hal-02110530

HAL Id: hal-02110530
https://hal.science/hal-02110530

Submitted on 7 Nov 2019

HAL is a multi-disciplinary open access archive for the deposit and dissemination of scientific research documents, whether they are published or not. The documents may come from teaching and research institutions in France or abroad, or from public or private research centers.

L'archive ouverte pluridisciplinaire **HAL**, est destinée au dépôt et à la diffusion de documents scientifiques de niveau recherche, publiés ou non, émanant des établissements d'enseignement et de recherche français ou étrangers, des laboratoires publics ou privés.

Distributed under a Creative Commons Attribution - NonCommercial - NoDerivatives 4.0 International License

*Revised Manuscript with no changes marked
Click here to view linked References

Impact of spatial variability in hydraulic parameters on plume migration within unsaturated surficial formations

Léa Pannecoucke[a,*], Mathieu Le Coz[b], Clémence Houzé[c], Albane Saintenoy[c], Charlotte Cazala[b], Chantal de Fouquet[a]

[a]*MINES ParisTech, PSL University, Centre de Géosciences, 35 rue St Honoré, 77300 Fontainebleau, France*
[b]*Institut de Radioprotection et de Sûreté Nucléaire (IRSN), PSE-ENV/SEDRE, 31 avenue de la Division Leclerc, 92260 Fontenay-aux-Roses, France*
[c]*GEOPS, Univ. Paris-Sud, CNRS, Université Paris-Saclay, 91405 Orsay, France*

Abstract

Heterogeneities in textural properties of surficial formations at field scale result in spatial variations in hydraulic parameters governing unsaturated zone flow. This study aims at quantifying the influence of such variations on solute transport resulting from a localized source of radioactive contaminant at ground level.

The study focuses on three hydraulic parameters related to the Mualem-van Genuchten formalism, namely the saturated hydraulic conductivity K_s, the parameter α inversely proportional to the air-entry value, and the parameter n related to the pore-size distribution. Sets of random fields accounting for spatial variability of these parameters are generated using lognormal distributions with different variances and correlation lengths. These random fields are used as inputs to an unsaturated flow and transport model to simulate radionuclide plume migration.

*Corresponding author: lea.pannecoucke@mines-paristech.fr

Each simulated plume is characterized by its size (plume surface area), position (location of center of mass) and shape (elongation ratio) within the unsaturated zone. By comparison with the homogeneous medium, K_s-, α- and n- random fields generated with the mean variances computed through the analysis of a global soil database respectively result in average in (i) 25 (variable K_s), 20 (variable α) and 65% (variable n) increase in plume size; (ii) 0.8, 1 and 1.8 m horizontal offsets of the plume center; and (iii) 20, 30 and 50% decrease in plume circularity. In addition, changes in the variance values within one order of magnitude appear to have critical consequences only for the n parameter.

The issue of spatial variability of hydraulic parameters is thus crucial for characterizing the evolution of pollutant plumes within an unsaturated zone and for developing better remediation strategies for industrial sites.
Keywords: Richards equation, Mualem-van Genuchten model, Random fields, Radionuclide migration, Sensitivity analysis.

1. Introduction

Spatial heterogeneities found in porous formations at field scale impact groundwater flow and solute transport. The role of geometrical patterns, especially connected features, in concentrating flow and reducing travel time has been widely highlighted, in both saturated (Knudby and Carrera, 2005; Renard and Allard, 2013) and unsaturated (Appels et al., 2018) zones. Most of the related studies assume that such patterns mainly result from the arrangement of large-scale discrete geological structures with high contrast in hydraulic parameters (Feyen and Caers, 2006; Ye and Khaleel, 2008). The spatial distribution of these parameters can be represented by either several unimodal random fields populating a discontinuous facies model (Matheron et al., 1987; Le Coz et al., 2011; Le Coz et al., 2013) or a single continuous random field whose properties are multimodal (Russo, 2012).

Smaller scale variability, *i.e.* within individual facies, is known to contribute significantly to the overall hydraulic parameters variability within the unsaturated zone (Botros et al., 2009). When considering such individual facies, the corresponding parameters are generally represented by a single population whose distribution is unimodal, more particularly lognormal for the hydraulic conductivity (Fogg et al., 1998; Paleologos et al., 2015; Tan et al., 2017), and whose spatial variability can be characterized through a two-point spatial covariance (Botros et al., 2009; Russo, 2012). However, identifying a relevant covariance model requires a large amount of data at field scale (*e.g.*, Botros et al., 2009) and is a complex task because the measurements of hydraulic parameters that govern unsaturated zone flow are difficult and time-consuming (Shaap et al., 2004).

The spatial variability within individual facies is thus often neglected, for instance in most of the studies that focus on the spread of radioactive contaminants in the unsaturated zone (Skuratovič et al., 2016; Testoni et al., 2017). In particular, Testoni et al. (2017) simulated the barrier effect of the unsaturated zone as a delay and capture system by considering various medium configurations and initial conditions in case of an accidental release of Cesium 137. These simulations were performed by coupling of (i) a distributed one-dimensional unsaturated flow and transport model and (ii) a three-dimensional saturated flow and transport model. This coupling is thus based on the assumption that the unsaturated water flow is mainly in the vertical direction. This commonly formulated assumption (Bugai et al., 2012; Jakimavičiūtė-Maselienė et al., 2016) is questionable since anisotropy induced by lateral variability in hydraulic parameters can refract flow lines away from vertical (Gannon et al., 2017).

This study aims at quantifying the influence of the spatial variability in hydraulic parameters on plume migration in unsaturated surficial formations, within the framework of a punctual release of radionuclides to the subsurface. First, the degree of spatial variability in hydraulic parameters at field scale, for typical soils, is assessed based on the analysis of a global soil database. Then, numerical simulations are run using a full two-dimensional (2D) flow and transport model to reproduce lateral flow induced by such spatial variability.

2. Unsaturated flow in porous media

This section recalls the main parameters governing flow in unsaturated surficial formations and quantifies their spatial variability in natural environment. The variance of three of these parameters is computed at field scale based on soil texture information recorded in a global soil database.

2.1. Governing equation and parameterization

Variably saturated flow processes in porous media are typically described by the Richards equation:

$$\frac{\partial \theta(\psi)}{\partial t} = \nabla.(K(\psi)\nabla(\psi + z)) + q_{ss} \tag{1}$$

where θ is the volumetric moisture content [$L^3.L^{-3}$], t is the time [T], K is the hydraulic conductivity tensor [$L.T^{-1}$], ψ is the water pressure head [L], z is the vertical coordinate directed upward [L] and q_{ss} represents distributed source (positive) or sink (negative) terms [$L^3.L^{-3}.T^{-1}$]. Solving the Richards equation requires the moisture retention curve and the relative hydraulic conductivity function as inputs describing the links between pressure head, water content and relative hydraulic conductivity. These relationships are based on a model, *e.g.*, the Mualem-van Genuchten model (Mualem, 1976; van Genuchten, 1980):

$$\theta(\psi) = \theta_r + \frac{\theta_s - \theta_r}{(1 + |\alpha\psi|^n)^m} \qquad \text{with} \qquad m = 1 - \frac{1}{n} \tag{2}$$

and

$$K(\psi) = K_s S_e^{\frac{1}{2}} [1 - (1 - S_e^{\frac{1}{m}})^m]^2 \qquad \text{with} \qquad S_e = \frac{\theta(\psi) - \theta_r}{\theta_s - \theta_r} \tag{3}$$

where θ_r and θ_s are respectively the residual and saturated volumetric water contents [$L^3.L^{-3}$], α is inversely proportional to the of air-entry value [L^{-1}], n is a pore-size distribution index [-] and K_s is the saturated hydraulic conductivity tensor [$L.T^{-1}$].

Although the hydraulic parameters are linked to physical soil properties, the direct measurement of some of them from samples is subject to experimental limitations (Schaap et al., 2004). Many investigations are thus undertaken to estimate hydraulic parameters using empirical relationships deduced from more readily available data, such as soil texture and bulk density (*e.g.*, Wösten et al., 1999; Schaap et al., 2001; Saxton and Rawls, 2006; Tóth et al., 2015; Zhang and Schaap, 2017). These relationships, commonly referred as pedotransfer functions (PTFs), are mostly based on regression analysis of existing soil databases. The ROSETTA PTF (Schaap et al., 2001) is based on artificial neural network analysis coupled with bootstrap re-sampling which allows to estimate hydraulic parameters of the Mualem-van Genuchten model.

The parameter θ_r can be quite precisely derived from soil texture using PTFs (Vereecken et al., 1989); both θ_r and θ_s can be directly obtained from measurements under extremely dry or saturated conditions at the subsurface respectively (Jadoon et al., 2012). In addition, preliminary sensitivity analyses performed in temperate climate conditions show that the spatial variability of these two parameters does not significantly influence the solute transport. The sensitivity analysis conducted in this study thus only focuses on the K_s, α and n parameters.

2.2. Variability of hydraulic parameters at field scale

2.2.1. Database analysis

The World Soil Information Service (WoSIS) aims at providing consistent harmonized (*i.e.*, georeferenced, quality-assessed and standardized) soil data on a global scale based on soil profiles compiled by the International Soil Reference and Information Center (ISRIC). The WoSIS database currently contains some 96,000 georeferenced soil profiles, described in terms of analytical and physical soil properties, among which 20% were so far quality-assessed and standardized (Batjes et al., 2017). The number of recorded data for each property varies between profiles; yet a majority of samples is described at least in term of soil texture, *i.e.* sand, silt and clay contents. These textural properties are thus used to estimate the Mualem-van Genuchten hydraulic parameters by mean of the ROSETTA PTF. The soil profiles from the WoSIS database are then grouped by locations. A location is defined as a circular area of radius 500 m that contains at least 10 soil profiles. For each of the 49 identified locations, the mean (μ) and variance (σ^2) of logK_s, logα and log$n$ (the parameters K_s, α and n are assumed to follow lognormal distributions) are computed based on the whole corresponding soil samples. The Pearson correlation coefficients (r) are also computed between the three parameter pairs, *i.e.*, logK_s and logα; logK_s and log$n$; and logα and log$n$.

2.2.2. Variances and correlations

On the 49 identified locations, the log-variances (which enables to work with a dimensionless parameter σ^2) of the hydraulic parameters generally vary within about one order of magnitude (Figure 1) in relation with the mean parameter values. Indeed, σ^2(logK_s) increases from 2.5.10^{-2} (1st decile) to 2.5.10^{-1} (9th decile) when $\mu(K_s)$ varies from 0.1 to 0.6 m.d^{-1}; σ^2(logα) decreases from 8.10^{-2} to 8.10^{-3} when $\mu(\alpha)$ varies from 0.9 to 2.7 m^{-1}; and σ^2(log$n$) increases from 8.10^{-4} to 1.10^{-2} when $\mu(n)$ varies from 1.25 to 1.65.

The Pearson correlation coefficients between the parameters also appear to depend on the mean parameter values (Figure 2). For $\mu(K_s)$ lower than 0.2 m.d^{-1}, r values are highly scattered: from -0.2 to 0.8 between logK_s and logα; from -0.7 to 0.9 between logK_s and log$n$; and from -0.9 to 0.5 between logα and log$n$. For $\mu(K_s)$ higher than 0.2 m.d^{-1}, r values are less scattered and tend to stabilize: from 0.3 to 0.7 between logK_s and logα; from 0.7 to 1 between logK_s and log$n$; and from -0.1 to 0.6 between logα and log$n$.

3. Methods

This section describes the modeling tools and approaches carried out for assessing the influence of spatial variability in K_s, α and n on the migration of a radionuclide plume in unsaturated surficial formations. A 2D hydrogeological flow and transport numerical model is run in simulation mode with various input parameter fields representing distinct levels of spatial variability.

3.1. Flow and transport numerical model

The MELODIE numerical code developed by the French Institute for Radiation Protection and Nuclear Safety (IRSN) aims at making available a tool for evaluating the long term safety of a radioactive waste disposal facility (IRSN, 2009; Amor et al., 2014; Amor et al., 2015; Bouzid et al., 2018). This code simulates underground flow and solute transport in saturated or variably saturated porous media based on a mixed finite volume - finite element scheme, namely, Godunov development for the convective term and Galerkin development for the diffusion - dispersion term (Amaziane et al., 2008). In this study, MELODIE is set for solving in 2D (i) the Richards equation describing flow in variably saturated porous media (Eq. 1); and (ii) the following advection-dispersion-reaction equation representing the migration of radionuclides:

$$\nabla.[(D|\overrightarrow{u}| + \omega d)\nabla C - \overrightarrow{u}C] = \omega' R\frac{\partial C}{\partial t} + \omega' \lambda RC \qquad (4)$$

where C is the volumetric radionuclide concentration [M.L^{-3}], D is the dispersivity tensor [L], d is the molecular diffusion coefficient [L^2.T^{-1}], $\overrightarrow{u}$ is the pore water velocity [L.T^{-1}], ω and ω' are respectively total and effective porosities [-], λ is the decay constant [T^{-1}] and R is the retardation factor [-].

The modeling domain (Figure 3a) consists of a 2D vertical section of surficial deposits of 100 m large (x axis) by 15 m deep (z axis), discretized in triangles of base 0.5 m and height 0.25 m. The boundary conditions are defined as follows:

1. a fixed head corresponding to the mean water table elevation (7.5 m above the bottom boundary with a 0.004 m.m^{-1} lateral gradient) is set on both sides of the domain;
2. no-flow conditions are set on the bottom boundary;
3. a time variable flow corresponding to the daily percolation rate, typical from center of France, and estimated from the water balance method (Thornthwaite and Mather, 1955) is imposed on the top boundary (Figure 3b).

A point source of tritium is simulated by setting an activity of 1,000 Bq.d^{-1} during one month on the top surface node located at the center of the modeling domain. The evolution of the activity within the domain is then simulated during six years with an adaptative time stepping (from 10^{-20} to 1 day) by considering a retardation factor (R) of 1 and a decay constant (λ) of 1.54.10^{-4} d^{-1} (Table 1). The tritium plume is delimited by the nodes for which the simulated activity is higher than 1 Bq.m$^{-3}{}_{H_2O}$.

3.2. Parameter fields

First, the internal model parameters are fixed homogeneously for the whole domain as representative of sandy loam material (Table 2). Then, sets of 100 simulations are run by considering (i) one hydraulic parameter (either K_s or α or n) variable in space through sets of 100 random fields with similar properties (*i.e.* same parameters used for the geostatistical simulations of random fields) and (ii) three hydraulic parameters (K_s and α and n) varying simultaneously through sets of 100 correlated random fields (Table 3).

Hereafter, Z is a random field referring indifferently to one of the hydraulic parameters under consideration. Since K_s, α and n are assumed to follow lognormal distributions, the logarithm of Z is a gaussian random field such that :

$$\log Z \sim \mathcal{N}(\mu, \sigma^2) \tag{5}$$

where μ and σ^2 are the mean and variance of $\log Z$, respectively. The variogram chosen to account for the spatial variability of $\log Z$ is the spherical model, which was shown to fit experimental data of soil hydraulic parameters (Herbst et al., 2006; Botros et al., 2009; Bevington et al., 2016):

$$\gamma(h) = \begin{cases} \dfrac{3}{2}\dfrac{|h|}{\delta} - \dfrac{1}{2}\left(\dfrac{|h|}{\delta}\right)^3, & \text{if } |h| \leq \delta \\ 1, & \text{if } |h| > \delta \end{cases} \tag{6}$$

where $\gamma(h)$ is the variogram value for pairs of points separated by a distance $|h|$ and δ is the range (correlation length). In order to take into account the anisotropy of geologic structures, a geometric anisotropy with different ranges along the horizontal and vertical directions (namely δ_X and δ_Z) is introduced. The simulations of $\log Z$ are performed by keeping a constant hazard as far as possible. Thus, the following sensitivity analysis takes into account the effect of changes in simulation parameters, rather than the effect of random sampling (Nguyen et al., 2018).

Each set of 100 random fields is built with specific σ^2, δ_X and δ_Z values (Table 3) defined consistently to studies performed at field scale showing that a significant spatial correlation typically exists within distances ranging from a few meters to 20 m (Taskinen at al., 2008). Yet, the μ value is fixed so that the geometric mean of Z corresponds to the mean sandy loam properties (Table 2).

3.3. Sensitivity analyses

For each of the three hydraulic parameters under study, the sensitivity of the simulated tritium plume to the properties (σ^2, δ_X and δ_Z) of the 100 corresponding random fields is analyzed with regards to the following features (only the unsaturated zone is considered):

1. the surface area of the plume, defined as the number of grid cells with a volumic activity higher than 1 $\mathrm{Bq.m^{-3}}_{\mathrm{H_2O}}$;

2. the distance between the center of mass of each plume and the center of mass of the plume simulated in the homogeneous medium (where $\sigma^2(\log K_s) = \sigma^2(\log\alpha) = \sigma^2(\log n) = 0$);

3. the elongation ratio (a/b) of the equivalent ellipse (Figure 4), defined as the ellipse whose center coincides with the center of mass of the plume and whose semi-minor and semi-major axes lengths (namely a and b) are proportional to the eigen values of the inertia matrix.

The number of simulations is set to 100 to ensure that the averages of the previous features reach a stabilization. The modeling conditions (initial and boundary conditions, transient fluxes, source term) are similar for all the simulations (see section 3.1). Only the soil properties (σ^2, δ_X and δ_Z) differ from one simulation to another.

3.4. Additional tests

In order to assess the effect of both radionuclide type and soil texture, two additional tests are conducted by considering different model parameterizations:

1. the tritium (ideal groundwater tracer) is replaced with a reactive radionuclide (*e.g.*, ^{90}Sr) with a retardation factor (R) of 3 and a decay constant (λ) of 6.59.10^{-4} d^{-1} (Table 1);

2. the sandy loam mean properties are replaced with silty clay loam mean properties, *i.e.* related to significantly finer texture (Table 2).

4. Results

This section presents the results averaged over each set of simulations for the last modeling time step, *i.e.* six years after the radionuclide injection. In order to assess the influence of the variance of hydraulic parameters on the plume features, the focus is first put on simulations with one hydraulic parameter varying (Table 3, sets 1., 2., 3.) and then on simulations with the three parameters varying simultaneously (Table 3, sets 4.). Then, the influence of the range values is described.

4.1. Sensitivity to the variance of one hydraulic parameter

Whatever the hydraulic parameter under consideration (K_s or α or n), the increase in the variance of the corresponding random field results both in the increase in the average plume surface areas (from 220, corresponding to the homogeneous plume, to 350 grid cells) and in the variability of this surface areas (standard deviation ranging from 0, corresponding to the homogeneous plume, to 110 grid cells) among the simulated plumes (Figure 5). The relationships between σ^2 and the surface areas of the plumes appear to be similar for the three hydraulic parameters under study when considering $\sigma^2(\log K_s)/\sigma^2(\log n) = 200$ and $\sigma^2(\log K_s)/\sigma^2(\log\alpha) = 5$.

In addition, the increase in variance for any hydraulic parameter results in the increase of the offset in both directions of the mean center of mass regarding the center of the homogeneous plume (Figure 6). The trend is yet stronger in the horizontal direction (mean offsets ranging from 0.5 to 2 m) than in the vertical direction (offsets ranging from 0.5 to 0.7 m). Besides, the relationships between σ^2 and the offsets are similar when considering $\sigma^2(\log K_s)/\sigma^2(\log n) = 200$ and $\sigma^2(\log K_s)/\sigma^2(\log\alpha) = 5$.

Finally, the increase in variance results in the decrease of the elongation ratio (from 0.88, corresponding to the homogeneous plume, to 0.45), regardless of which hydraulic parameter is considered (Figure 7). Thus, when the variability of hydraulic parameters is high, pollutant plumes are more likely to have an elongated shape. Besides, the relationships between σ^2 and the offsets are similar when considering $\sigma^2(\log K_s)/\sigma^2(\log n) = 200$ and $\sigma^2(\log K_s)/\sigma^2(\log\alpha) = 5$.

4.2. Sensitivity to the variance of the three hydraulic parameters

The mean and standard deviation of the plume surface areas, the mean offsets between each centers and the homogeneous center and the mean elongation ratios are computed for sets of 100 simulations with the three parameters varying simultaneously and in a correlated manner, with $\sigma^2(\log K_s)/\sigma^2(\log n) = 200$ and $\sigma^2(\log K_s)/\sigma^2(\log\alpha) = 5$.

These features are close to the values obtained for the sets with only one parameter varying, considering the corresponding variances (Figures 5, 6 and 7). Here, the results are given for a coefficient r of 0.8. Other values of r coefficient have been tested and lead to similar results.

4.3. Sensitivity to the ranges

Given the values of σ^2, δ_X and δ_Z chosen for this sensitivity analysis, the range in the horizontal direction (δ_X) does not seem to have a significant influence on the simulated plume features (size, center of mass and shape), regardless of which hydraulic parameter is considered (Figure 8). The influence of the range in the vertical direction (δ_Z) appears to be slightly more visible (Figure 9), especially regarding the mean plume surface areas and the location of the mean centers of mass: when the vertical range increases from 1 to 5 m, the mean plume surface areas decrease, especially for K_s and n (diminution from 300 to 250 and from 290 to 260 grid cells respectively) and the horizontal offsets regarding the homogeneous plume center increase of around 0.3 m for the three hydraulic parameters.

4.4. Additional tests

When considering a reactive radionuclide ($R = 3$), the simulated plumes are logically less developed than for the ideal groundwater tracer ($R = 1$). However, both the surface area and the related standard deviation increase significantly when the variance of each of the three hydraulic parameters considered increase. These features tend to stabilize when the average surface reaches about 130% of the surface simulated in a homogenous medium, consistently with the results for tritium (Figure 10).

The results obtained with mean hydraulic parameters related to a finer texture (silty clay loam) are similar to those above presented for sandy loam (Figure 10a). This could be explained by the fact that silty clay loam mean properties remain sufficiently favorable for leading the infiltration of the water height imposed at the top surface of the model (Figure 3b). The standard deviation computed for highest variances of the hydraulic parameters is yet lower (Figure 10b). This could be explained by the fact that a large distribution of the hydraulic parameters centered on sandy loam material could result in very high hydraulic conductivity values more favorable to the development of preferential flow paths and therefore to the lateral migration of the plume.

5. Discussion

This study allows to quantify the impact of the variance of the random fields representing the logarithms of the hydraulic parameters K_s, α and n on solute transport within unsaturated surficial formations. By focusing on variances estimated for porous media in natural environment at field scale, it appears that the n and, in a lesser extent, K_s parameters are the most critical (Figures 5, 6 and 7). Thus, by comparison with homogeneous parameter fields, random fields generated with $\sigma^2(\log K_s) = 0.14$, $\sigma^2(\log\alpha) = 0.036$ and $\sigma^2(\log n) = 0.005$, *i.e.* mean variances calculated based on the WoSIS database, respectively result in (i) 25, 20 and 65% increase in plume size;

(ii) 0.8, 1 and 1.8 m horizontal offsets of the plume center; and (iii) 20, 30 and 50% decrease in plume circularity. Besides, within the range of variation of $\sigma^2(\log n)$, the average surface areas range from 260 to 350 grid cells. In comparison, within the range of variation of $\sigma^2(\log K_s)$ and $\sigma^2(\log\alpha)$, the mean surface areas only range from 235 to 290, which highlights that n is the most critical parameter. Such results are consistent with previous studies showing the high influence of the spatial variability of the parameter n on flow (Lu and Zhang, 2002 and Tan et al., 2017) in the unsaturated zone.

This study also shows that the simulated plumes are far less sensitive to changes in ranges than changes in variances of the random fields representing the hydraulic parameters, at least for the intervals of values chosen. Yet, the impact of the vertical range appears to be more pronounced than the horizontal range: when the zones of high or low values of hydraulic parameters are more expanded in depth (higher value of vertical ranges), the preferential flow paths are potentially more continuous and the plume surface areas tend to decrease and get closer to the homogeneous plume surface area. The values of horizontal ranges considered here are of the same order of magnitude as the pollutant plumes extensions (a few meters): it could explain the low influence of the changes in horizontal range on the simulated plumes. Nevertheless, these ranges are consistent with analyses of soil parameter variability at field scale (Russo et al., 1997 and Botros et al., 2009). However, for higher values of ranges (from hundreds of meters to a thousand meter), the influence of horizontal range on the flow rate in unsaturated zone was shown to be more significant (Tan et al., 2017).

The sensitivity analysis performed in this study mainly focuses on an ideal groundwater tracer (tritium) in sandy texture. However, additional tests show that the results obtained for reactive radionuclides and a finer texture are comparable (at least for similar infiltration rate). From a general standpoint, this study thus indicates that taking into account the weak intra-facies (small scale) spatial variability is critical for characterizing plume migration within unsaturated zone. This requires to develop in-situ approaches for estimating more efficiently soil hydraulic parameters and their variability at field scale (*e.g.*, Léger et al., 2014; Léger et al., 2016). When these parameters remain poorly recognized, a set of simulations based on typical variability deduced from local or global database can be used for identifying the plume properties and the related uncertainties at a given time.

6. Conclusion

This work has highlighted the critical influence of the spatial variability in hydraulic parameters, in particular pore-size distribution index (n), on radionuclide migration in unsaturated surficial formations. In practice, this work demonstrates the need for well characterizing this spatial variability in order to quantify and locate soil volumes that need to be removed or depolluted in the context of remediation of nuclear or industrial sites. It also quantifies the corresponding uncertainties.

In addition, although the quantitative results presented in this paper are related to a theoretical example and are dependent on the model settings (environmental parameters, radionuclide, etc.), the proposed method (random field generation, physically-based groundwater transport simulations, plume properties characterization) can be transposed to other contexts, such as chemical pollutions or design of devices to contain pollutant spread.

Acknowledgements

This study is part of *Kri-Terres* project, supported by the French National Radioactive Waste Management Agency (ANDRA) under the French "Investments for the Future" Program. The authors are also grateful to Xavier Freulon (MINES ParisTech), Jean-Charles Robinet (ANDRA) and Marc Bourgeois (IRSN) for their helpful advices. We also thank two anonymous reviewers and the Associate Editor for their constructive suggestions.

References

Amaziane, B., El Ossmani, M., Serres, C., 2008. Numerical modeling of the flow and transport of radionuclides in heterogeneous porous media. Computational Geosciences 12 (4), 437–449.

Amor, H., Bourgeois, M., Le, M.-H., 2014. Development of an Adaptive Mesh Refinement strategy for the Melodie software simulating flow and radionuclide transport in porous media. In: NM2 PorousMedia, October 3, 2014. Dubrovnik, Croatia.

Amor, H., Benkhaldoun, F., Bourgeois, M., Le, M.-H., 2015. Development of an adaptive mesh refinement strategy for the MELODIE software simulating flow and radionuclides transport in heterogeneous porous media. In: MAMERN VI2015 Conference, June 1-5, 2015. Pau, France.

Appels, W. M., Ireson, A. M., Barbour, S. L., 2018. Impact of bimodal textural heterogeneity and connectivity on flow and transport through unsaturated mine waste rock. Advances in Water Resources 112, 254–265.

Batjes, N. H., Ribeiro, E., van Oostrum, A., Leenaars, J., Hengl, T., Mendes de Jesus, J., 2017. WoSIS: providing standardised soil profile data for the world. Earth System Science Data 9 (1), 1–14.

Bevington, J., Piragnolo, D., Teatini, P., Vellidis, G., Morari, F., 2016. On the spatial variability of soil hydraulic properties in a Holocene coastal farmland. Geoderma 262, 294–305.

Botros, F. E., Harter, T., Onsoy, Y. S., Tuli, A., Hopmans, J. W., 2009. Spatial Variability of Hydraulic Properties and Sediment Characteristics in a Deep Alluvial Unsaturated Zone. Vadose Zone Journal 8 (2), 276–289.

Bouzid, M., Espivent, C., Bourgeois, M., Amor, H., Marsal, F., 2018. Numerical modelling of radionuclide migration in the context of a near-surface LILW disposal facility. In: WM2018 Conference, March 18-22, 2018. Phoenix, Arizona, USA.

Bugai, D., Skalskyy, A., Dzhepo, S., Kubko, Y., Kashparov, V., Van Meir, N., Stammose, D., Simonucci, C., Martin-Garin, A., 2012. Radionuclide migration at experimental polygon at Red Forest waste site in Chernobyl zone. Part 2: Hydrogeological characterization and groundwater transport modeling. Applied Geochemistry 27 (7), 1359–1374.

Feyen, L., Caers, J., 2006. Quantifying geological uncertainty for flow and transport modeling in multi-modal heterogeneous formations. Advances in Water Resources 29 (6), 912–929.

Fogg, G. E., Noyes, C. D., Carle, S. F., 1998. Geologically based model of heterogeneous hydraulic conductivity in an alluvial setting. Hydrogeology Journal 6 (1), 131–143.

Gannon, J. P., McGuire, K. J., Bailey, S. W., Bourgault, R. R., Ross, D. S., 2017. Lateral water flux in the unsaturated zone: A mechanism for the formation of spatial soil heterogeneity in a headwater catchment. Hydrological Processes 31 (20), 1–12.

Herbst, M., Diekkrüger, B., Vereecken, H., 2006. Geostatistical co-regionalization of soil hydraulic properties in a micro-scale catchment using terrain attributes. Geoderma 132 (1), 206–221.

IRSN, 2009. MELODIE Modèle d'Evaluation à LOng terme des Déchets Irradiants Enterrés. Notice théorique du code de calcul MELO version 5.0. (in french).

Jadoon, K. Z., Weihermüller, L., Scharnagl, B., Kowalsky, M. B., Bechtold, M., Hubbard, S. S., Vereecken, H., Lambot, S., 2012. Estimation of Soil Hydraulic Parameters in the Field by Integrated Hydrogeophysical Inversion of Time-Lapse Ground-Penetrating Radar Data. Vadose Zone Journal 11 (4).

Jakimavičiūtė-Maselienė, V., Mažeika, J., Motiejūnas, S., 2016. Application of vadose zone approach for prediction of radionuclide transfer from near-surface disposal facility. Progress in Nuclear Energy 88, 53–57.

Knudby, C., Carrera, J., 2005. On the relationship between indicators of geostatistical, flow and transport connectivity. Advances in Water Resources 28 (4), 405–421.

Le Coz, M., Favreau, G., Ousmane, S. D., 2013. Modeling increased groundwater recharge due to change from rainfed to irrigated cropping in a semiarid region. Vadose Zone Journal 12 (2), 1–12.

Le Coz, M., Genthon, P., Adler, P. M., 2011. Multiple-Point Statistics for Modeling Facies Heterogeneities in a Porous Medium: The Komadugu-Yobe Alluvium, Lake Chad Basin. Mathematical Geosciences 43 (7), 861–878.

Léger, E., Saintenoy, A., Coquet, Y., 2014. Hydrodynamic parameters of a sandy soil determined by ground-penetrating radar inside a single ring infiltrometer. Water Resources Research 50 (7), 5459–5474.

Léger, E., Saintenoy, A., Tucholka, P., Coquet, Y., 2016. Hydrodynamic Parameters of a Sandy Soil Determined by Ground-Penetrating Radar Monitoring of Porchet Infiltrations. IEEE Journal of Selected Topics in Applied Earth Observations and Remote Sensing 9 (1), 188–200.

Lu, Z., Zhang, D., 2002. Stochastic analysis of transient flow in heterogeneous, variably saturated porous media: the van Genuchten-Mualem constitutive model. Vadose Zone Journal 1, 137–149.

Matheron, G., Beucher, H., de Fouquet, C., Galli, A., Guerillot, D., Ravenne, C., 1987. Conditional Simulation of the Geometry of Fluvio-Deltaic Reservoirs. In: SPE Annual Technical Conference and Exhibition, September 27-30, 1987. Society of Petroleum Engineers, Dallas, Texas, USA.

Mualem, Y., 1976. A new model for predicting the hydraulic conductivity of unsaturated porous media. Water Resources Research 12 (3), 513–522.

Nguyen, H. L., de Fouquet, C., Courbet, C., Gurriaran, R., Kashparov, V., Levchuk, S., Barker, 2018. Analysis of the relationship binding in situ gamma count rates and soil sample activities: Implication on radionuclide inventory and uncertainty estimates due to spatial variability. Journal of Environmental Radioactivity 192, 349–361.

Paleologos, E. K., Papapetridis, K., Kendall, C. G. S. C., 2015. Stochastic contaminant transport monitoring in heterogeneous sand and gravel aquifers of the United Arab Emirates. Stochastic Environmental Research and Risk Assessment 29 (5), 1427–1435.

Renard, P., Allard, D., 2013. Connectivity metrics for subsurface flow and transport. Advances in Water Resources 51, 168–196.

Russo, D., 2012. Numerical analysis of solute transport in variably saturated bimodal heterogeneous formations with mobileimmobile-porosity. Advances in Water Resources 47, 31–42.

Russo, D., Russo, I., Laufer, A., 1997. On the spatial variability of parameters of the unsaturated hydraulic conductivity. Water Resources Research 33 (5), 947–956.

Saxton, K. E., Rawls, W. J., 2006. Soil water characteristic estimates by texture and organic matter for hydrologic solutions. Soil Science Society of America Journal 70 (5), 1569–1578.

Schaap, M. G., Leij, F. J., van Genuchten, M. T., 2001. ROSETTA: a computer program for estimating soil hydraulic parameters with hierarchical pedotransfer functions. Journal of Hydrology 251, 163–176.

Schaap, M. G., Nemes, A., van Genuchten, M. T., 2004. Comparison of Models for Indirect Estimation of Water Retention and Available Water in Surface Soils. Vadose Zone Journal 3 (4), 1455–1463.

Skuratovič, Z., Mažeika, J., Petrošius, R., Martma, T., 2016. Investigations of the unsaturated zone at two radioactive waste disposal sites in Lithuania. Isotopes in Environmental and Health Studies 52 (4-5), 544–552.

Tan, X., Wang, X., Khoshnevisan, S., Hou, X., Zha, F., 2017. Seepage analysis of earth dams considering spatial variability of hydraulic parameters. Engineering Geology 228, 260–269.

Taskinen, A., Sirviö, H., Bruen, M., 2008. Modelling effects of spatial variability of saturated hydraulic conductivity on autocorrelated overland flow data: linear mixed model approach. Stochastic Environmental Research and Risk Assessment 22 (1), 67–82.

Testoni, R., Levizzari, R., De Salve, M., 2017. Coupling of unsaturated zone and saturated zone in radionuclide transport simulations. Progress in Nuclear Energy 95, 84–95.

Thornthwaite, C. W., Mather, J. R., 1955. The water balance. Publications in climatology 8, 1–104.

Tóth, B., Weynants, M., Nemes, A., Makó, A., Bilas, G., Tóth, G., 2015.

New generation of hydraulic pedotransfer functions for Europe. European Journal of Soil Science 66 (1), 226–238.

van Genuchten, M. T., 1980. A closed-form equation for predicting the hydraulic conductivity of unsaturated soils. Soil Science Society of America Journal 44 (5), 892–898.

Vereecken, H., Maes, J., Feyen, J., Darius, P., 1989. Estimating the soil moisture retention characteristic from texture, bulk density, and carbon content. Soil Science 148 (6), 389.

Wösten, J. H. M., Lilly, A., Nemes, A., Le Bas, C., 1999. Development and use of a database of hydraulic properties of European soils. Geoderma 90 (3), 169–185.

Ye, M., Khaleel, R., 2008. A markov chain model for characterizing medium heterogeneity and sediment layering structure. Water Resources Research 44 (9), W09427.

Zhang, Y., Schaap, M. G., 2017. Weighted recalibration of the Rosetta pedotransfer model with improved estimates of hydraulic parameter distributions and summary statistics (Rosetta3). Journal of Hydrology 547, 39–53.

Figure1
Click here to download high resolution image

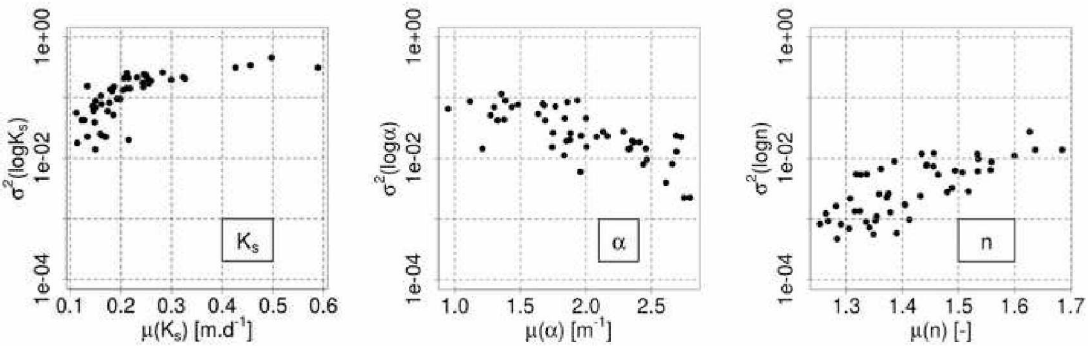

Figure2
Click here to download high resolution image

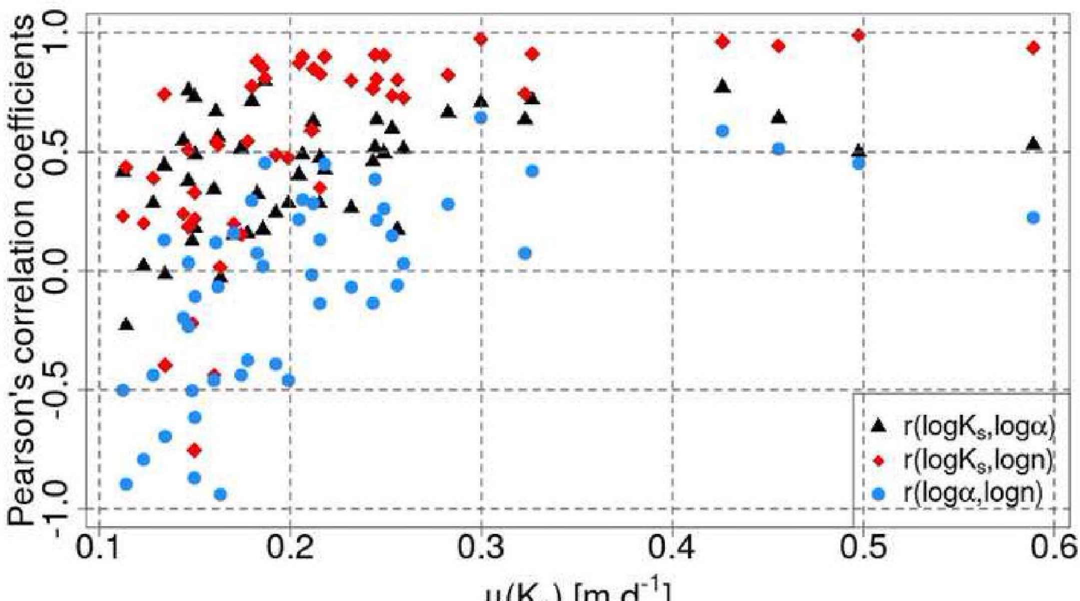

Figure3
Click here to download high resolution image

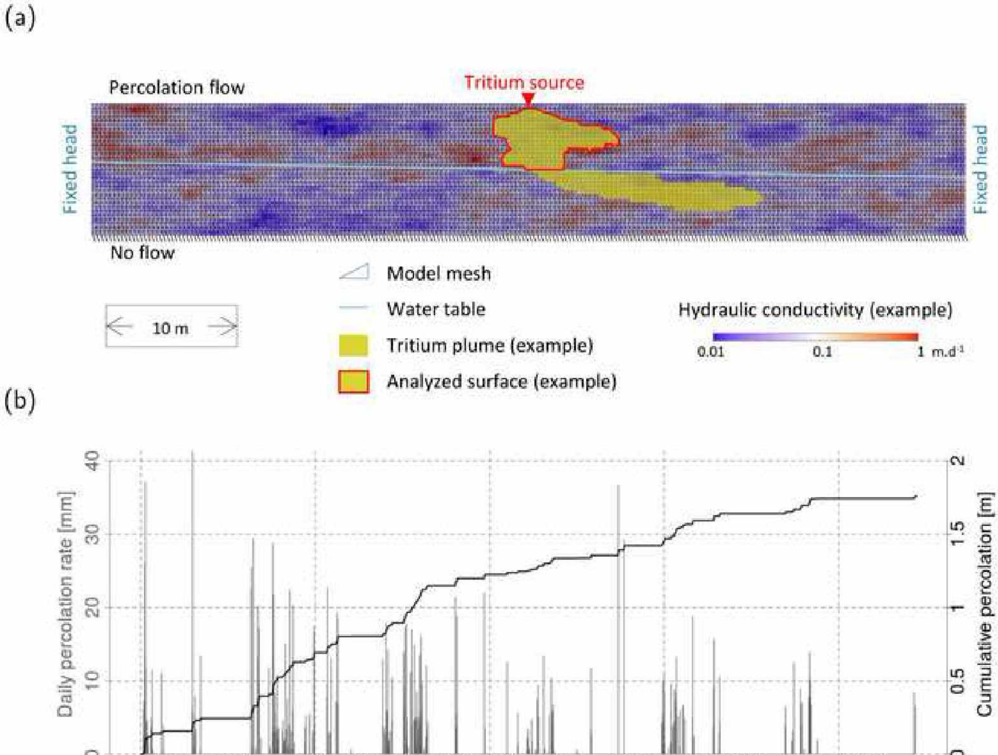

Figure4
Click here to download high resolution image

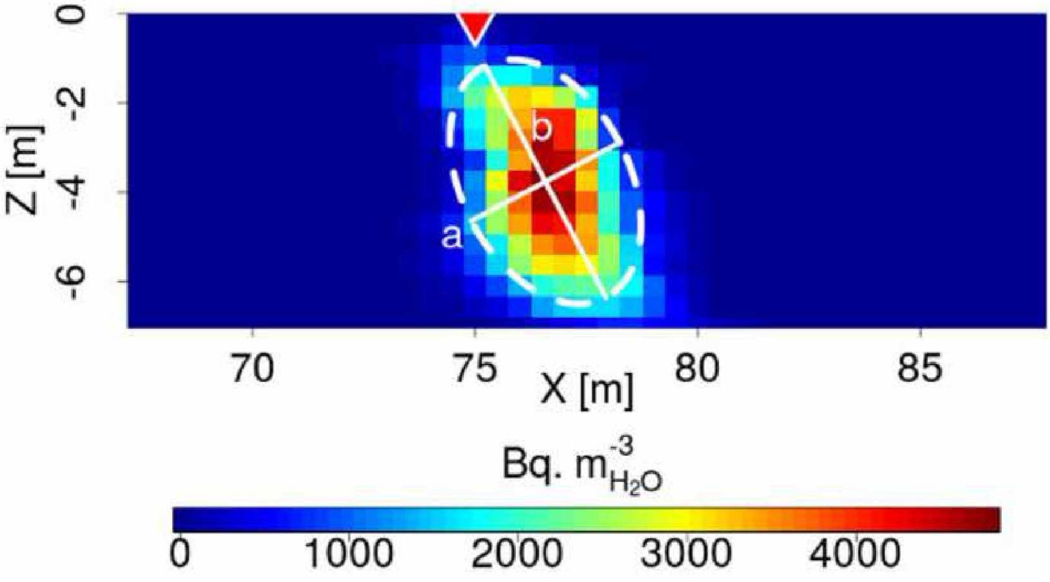

Figure5

Click here to download high resolution image

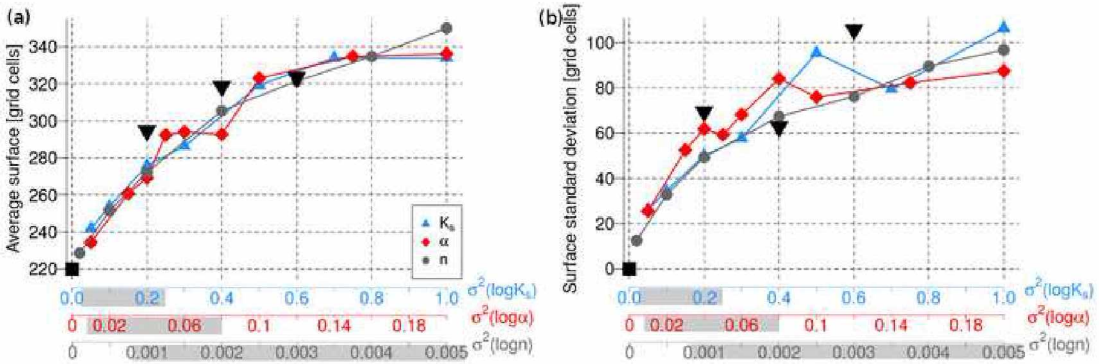

Figure6
Click here to download high resolution image

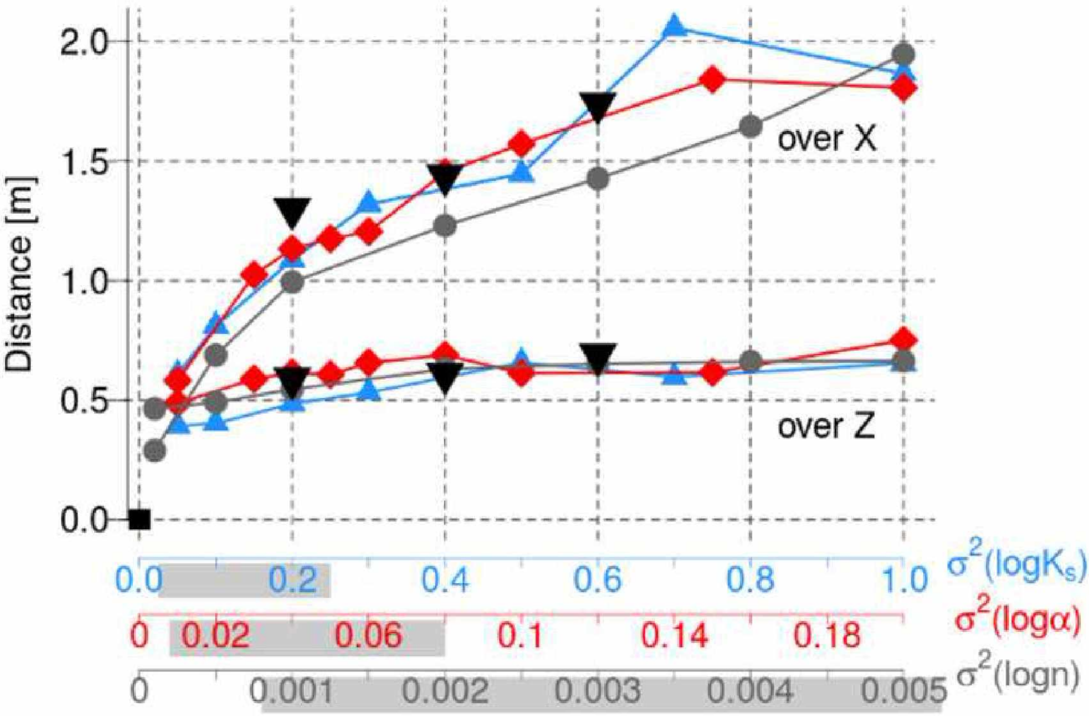

Figure7
Click here to download high resolution image

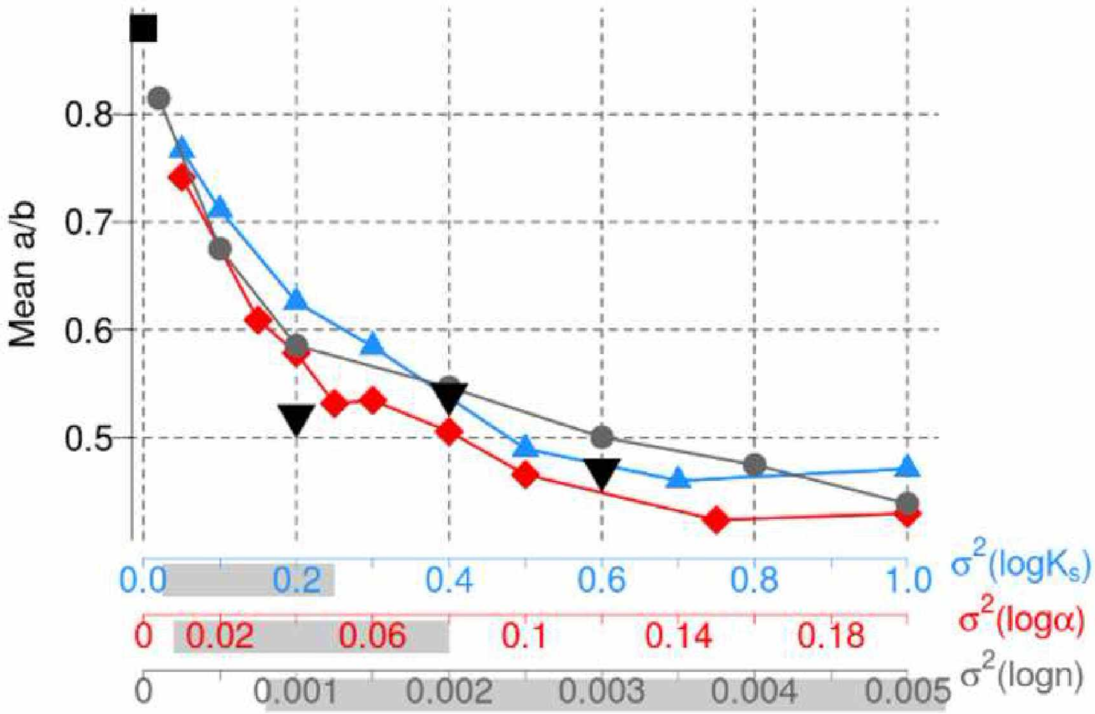

Figure8
Click here to download high resolution image

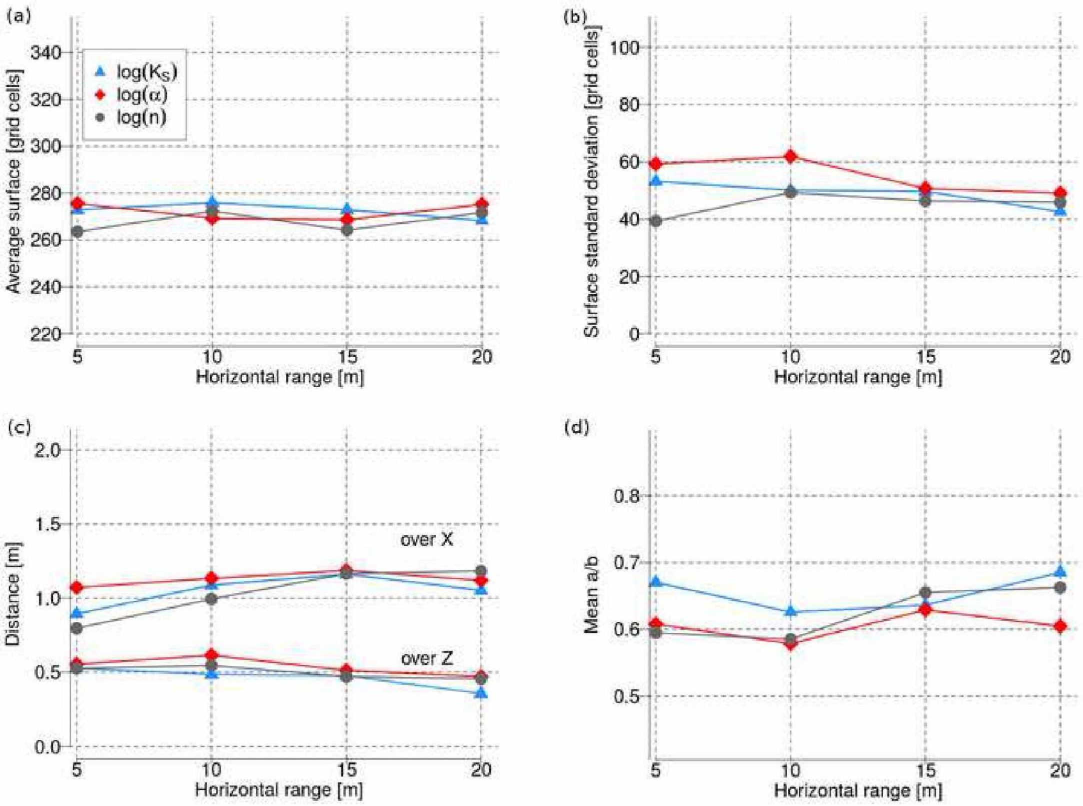

Figure9

Click here to download high resolution image

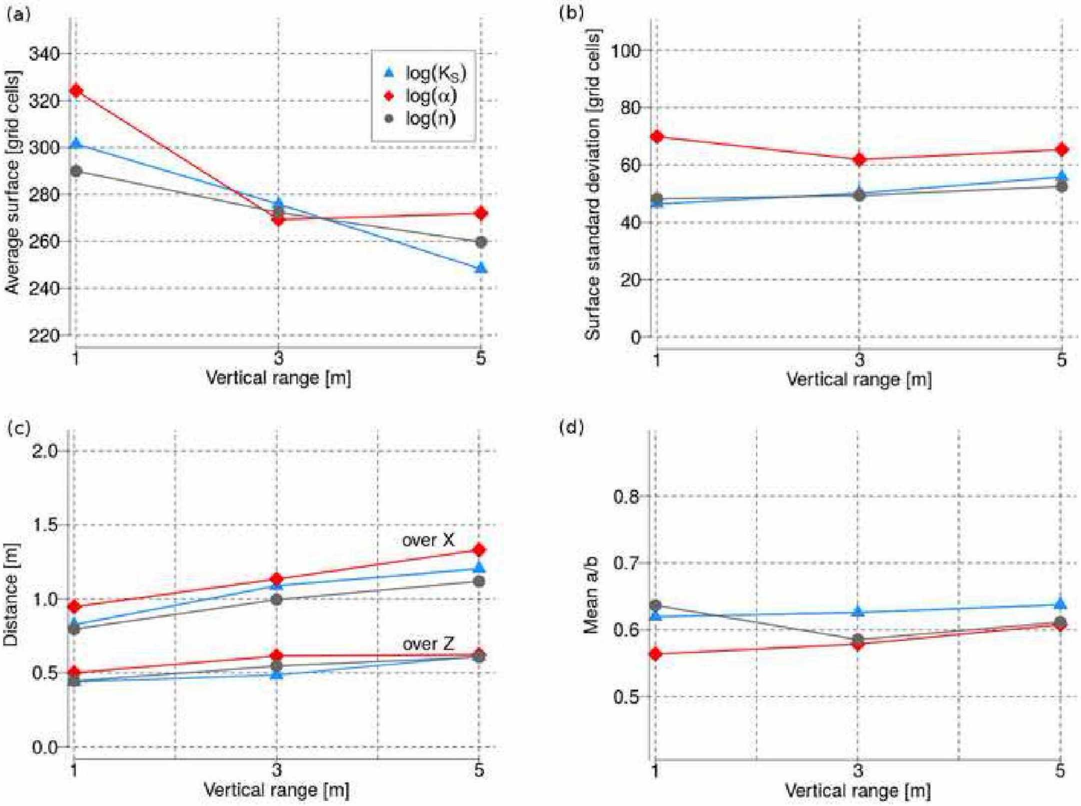

Figure10

Click here to download high resolution image

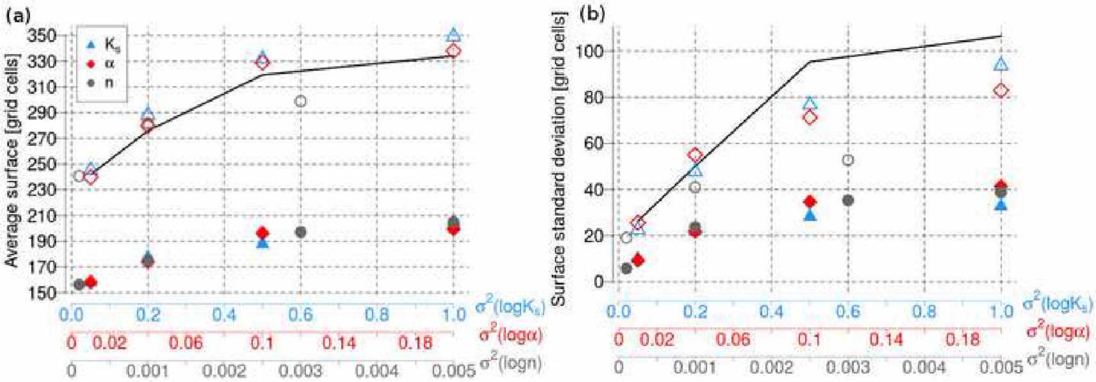

Figure captions

Figure 1: Log-variances in function of means for K_s, α and n for each location built via WoSIS database analysis.

Figure 2: Pearson's correlation coefficients between the log-parameters in function of $\mu(K_s)$ for each location built via WoSIS database analysis.

Figure 3: (a) Modeling domain with an example of hydraulic conductivity random field and resulting tritium plume. (b) Daily percolation rate and cumulative percolation rate used for the simulations.

Figure 4: Example of pollutant plume within the unsaturated zone with its equivalent ellipse in dotted line. The *a/b* ratio gives a hint about the elongation of the plume: the more *a/b* is close to 0, the more the plume has an elongated shape. The triangle highlights the tritium source.

Figure 5: Average plume surface areas (a) and standard deviation of surface areas (b) depending on σ^2 for the three hydraulic parameters. The squares correspond to the homogeneous medium and the three upside-down triangles on each graph correspond to media where the three hydraulic parameters are varying in a correlated manner. The values of δ_X and δ_Z are set to 10m and 3m. The shaded rectangles on the axes correspond to the range of variances found at field scale via WoSIS database.

Figure 6: Mean distances with the center of the plume simulated in the homogeneous medium in function of σ^2 for the three hydraulic parameters. The square corresponds to the homogeneous medium and the six upside-down triangles correspond to the media where the three hydraulic parameters are varying in a correlated manner. The values of δ_X and δ_Z are set to 10m and 3m. The shaded rectangles on the axes correspond to the range of variances found at field scale via WoSIS database.

Figure 7: Mean *a/b* ratio in function of σ^2 for the three hydraulic parameters. The square corresponds to the homogeneous medium and the three upside-down triangles correspond to the media where the hydraulic parameters are varying in a correlated manner. The values of δ_X and δ_Z are set to 10m and 3m. The shaded rectangles on the axes correspond to the range of variances found at field scale via WoSIS database.

Figure 8: Average (a) and standard deviation (b) of the plume surface areas depending on the horizontal range for the three hydraulic parameters. Average distances (c) with the homogeneous center and mean elongation ratio (d) in function of the horizontal range. The values of σ^2 are set to 0.2 for logK_s, 0.04 for logα and 0.001 for log$n$ and δ_Z is set to 3m.

Figure 9: Average (a) and standard deviation (b) of the plume surface areas depending on the vertical range for the three hydraulic parameters. Average distances (c) with the homogeneous center and mean elongation ratio (d) in function of the vertical range. The values of σ^2 are set to 0.2 for logK_s, 0.04 for logα and 0.001 for log$n$ and δ_X is set to 10m.

Figure 10: Average (a) and standard deviation (b) of the plume surface areas depending on σ^2 for the three hydraulic parameters. The black line corresponds to the results obtained for tritium and sandy loam texture (for the parameter K_s). The filled symbols correspond to the results for the reactive radionuclide and sandy loam texture. The empty symbols correspond to the results for tritium and silty clay loam texture.

Table1 (revised)
Click here to download Table: table1.pdf

	ω [-]	D_z [m]	D_z [m]	d [m^2.d^{-1}]	λ [d^{-1}]	R [-]
Tritium	0.38	0.05	0.005	0.00001	$1.54.10^{-4}$	1
Reactive radionuclide	0.38	0.05	0.005	0.00001	$6.59.10^{-4}$	3

Table2 (revised)
Click here to download Table: table2.pdf

	θ_r [L^3.L^{-3}]	θ_s [L^3.L^{-3}]	K_s [m.d^{-1}]	α [m^{-1}]	n [-]	K_x/K_z [-]
Sandy loam	0.039	0.38	0.38	2.67	1.45	10
Silty clay loam	0.090	0.48	0.11	0.84	1.52	10

Table3
Click here to download Table: table3.pdf

	$\sigma^2(\log K_s)$	$\sigma^2(\log\alpha)$	$\sigma^2(\log n)$	δ_X [m]	δ_Z [m]	$r(\log K_s, \log\alpha)$ and $r(\log K_s, \log n)$
Set 1.1	0.05	0	0	10	3	-
Set 1.2	0.1	0	0	10	3	-
Set 1.3	0.2	0	0	5	3	-
Set 1.4	0.2	0	0	10	3	-
Set 1.5	0.2	0	0	15	3	-
Set 1.6	0.2	0	0	20	3	-
Set 1.7	0.2	0	0	10	1	-
Set 1.8	0.2	0	0	10	5	-
Set 1.9	0.3	0	0	10	3	-
Set 1.10	0.5	0	0	10	3	-
Set 1.11	0.7	0	0	10	3	-
Set 1.12	1	0	0	10	3	-
Set 2.1	0	0.01	0	10	3	-
Set 2.2	0	0.03	0	10	3	-
Set 2.3	0	0.04	0	5	3	-
Set 2.4	0	0.04	0	10	3	-
Set 2.5	0	0.04	0	15	3	-
Set 2.6	0	0.04	0	20	3	-
Set 2.7	0	0.04	0	10	1	-
Set 2.8	0	0.04	0	10	5	-
Set 2.9	0	0.05	0	10	3	-
Set 2.10	0	0.06	0	10	3	-
Set 2.11	0	0.08	0	10	3	-
Set 2.12	0	0.1	0	10	3	-
Set 2.13	0	0.15	0	10	3	-
Set 2.14	0	0.20	0	10	3	-
Set 3.1	0	0	0.0001	10	3	-
Set 3.2	0	0	0.0005	10	3	-
Set 3.3	0	0	0.001	5	3	-
Set 3.4	0	0	0.001	10	3	-
Set 3.5	0	0	0.001	15	3	-
Set 3.6	0	0	0.001	20	3	-
Set 3.7	0	0	0.001	10	1	-
Set 3.8	0	0	0.001	10	5	-
Set 3.9	0	0	0.002	10	3	-
Set 3.10	0	0	0.003	10	3	-
Set 3.11	0	0	0.004	10	3	-
Set 3.12	0	0	0.005	10	3	-
Set 4.1	0.2	0.04	0.001	10	3	0.8
Set 4.2	0.4	0.08	0.002	10	3	0.8
Set 4.3	0.6	0.12	0.003	10	3	0.8

Table captions (revised)

Table 1: Transport parameters used in (Eq. 4) for tritium and for a reactive radionuclide.

Table 2: Soil hydraulic (flow) parameters derived from ROSETTA PTF for sandy loam and silty clay loam materials, used in (Eq. 1), (Eq. 2) and (Eq. 3).

Table 3: Values of variances, ranges and Pearson's correlation coefficients for each set of 100 simulations.